

# CESA TRAFFICKING INHIBITOR Inhibits Cellulose Deposition and Interferes with the Trafficking of Cellulose Synthase Complexes and Their Associated Proteins KORRIGAN1 and POM2/CELLULOSE SYNTHASE INTERACTIVE PROTEIN1<sup>1</sup>[OPEN]

Natasha Worden, Thomas E. Wilkop, Victor Esteva Esteve, Richard Jeannotte, Rahul Lathe, Samantha Vernhettes, Bart Weimer, Glenn Hicks, Jose Alonso, John Labavitch, Staffan Persson, David Ehrhardt, and Georgia Drakakaki\*

Departments of Plant Sciences (N.W., T.E.W., V.E.E., J.L., G.D.) and Veterinary Medicine (R.J., B.W.), University of California, Davis, California 95616; Max-Planck-Institute of Molecular Plant Physiology, Science Campus, 14476 Golm, Germany (R.L., S.P.); Institut National de la Recherche Agronomique, Institute Jean-Pierre Bourgin, 78026 Versailles, France (S.V.); Department of Botany and Plant Sciences, University of California, Riverside, California 92521 (G.H.); Department of Plant and Microbial Biology, North Carolina State University, Raleigh, North Carolina 27695 (J.A.); Australian Research Council Centre of Excellence in Plant Cell Walls, School of Botany, University of Melbourne, Parkville, Victoria 3010, Australia (S.P.); and Department of Plant Biology, Carnegie Institution for Science, Stanford, California 94305 (D.E.)

ORCID ID: 0000-0002-0804-2884 (N.W.).

Cellulose synthase complexes (CSCs) at the plasma membrane (PM) are aligned with cortical microtubules (MTs) and direct the biosynthesis of cellulose. The mechanism of the interaction between CSCs and MTs, and the cellular determinants that control the delivery of CSCs at the PM, are not yet well understood. We identified a unique small molecule, CESA TRAFFICKING INHIBITOR (CESTRIN), which reduces cellulose content and alters the anisotropic growth of *Arabidopsis thaliana* hypocotyls. We monitored the distribution and mobility of fluorescently labeled cellulose synthases (CESAs) in live *Arabidopsis* cells under chemical exposure to characterize their subcellular effects. CESTRIN reduces the velocity of PM CSCs and causes their accumulation in the cell cortex. The CSC-associated proteins KORRIGAN1 (KOR1) and POM2/CELLULOSE SYNTHASE INTERACTIVE PROTEIN1 (CSI1) were differentially affected by CESTRIN treatment, indicating different forms of association with the PM CSCs. KOR1 accumulated in bodies similar to CESA; however, POM2/CSI1 dissociated into the cytoplasm. In addition, MT stability was altered without direct inhibition of MT polymerization, suggesting a feedback mechanism caused by cellulose interference. The selectivity of CESTRIN was assessed using a variety of subcellular markers for which no morphological effect was observed. The association of CESAs with vesicles decorated by the trans-Golgi network-localized protein SYNTAXIN OF PLANTS61 (SYP61) was increased under CESTRIN treatment, implicating SYP61 compartments in CESA trafficking. The properties of CESTRIN compared with known CESA inhibitors afford unique avenues to study and understand the mechanism under which PM-associated CSCs are maintained and interact with MTs and to dissect their trafficking routes in etiolated hypocotyls.

Plant cell expansion and anisotropic cell growth are driven by vacuolar turgor pressure and cell wall extensibility, which in a dynamic and restrictive manner direct cell morphogenesis (Baskin, 2005). Cellulose is

the major load-bearing component of the cell wall and is thus a major determinant for anisotropic growth (Baskin, 2001). Cellulose is made up of  $\beta$ -1,4-linked glucan chains that may aggregate to form microfibrils holding 18 to 36 chains (Somerville, 2006; Fernandes et al., 2011; Jarvis, 2013; Newman et al., 2013; Thomas et al., 2013). In contrast to cell wall structural polysaccharides, including pectin and hemicellulose, which are synthesized by Golgi-localized enzymes, cellulose is synthesized at the plasma membrane (PM) by cellulose synthase complexes (CSCs; Somerville, 2006; Scheller and Ulvskov, 2010; Atmodjo et al., 2013). The cellulose synthases (CESAs) are the principal catalytic units of cellulose biosynthesis and in higher plants are organized into globular rosettes (Haigler and Brown, 1986). For their biosynthetic function, each primary cell

<sup>1</sup> This work was supported by the National Science Foundation (grant nos. IOS-1258135 to G.D., DGE-0653984 to N.W., and DBI-0820755 to J.A.) and by the Deutsch Forschungsgemeinschaft (grant nos. PE1642/5-1 and DAAD [A/10/75281] to S.P. and R.L.).

\* Address correspondence to gdrakakaki@ucdavis.edu.

The author responsible for distribution of materials integral to the findings presented in this article in accordance with the policy described in the Instructions for Authors ([www.plantphysiol.org](http://www.plantphysiol.org)) is: Georgia Drakakaki (gdrakakaki@ucdavis.edu).

<sup>[OPEN]</sup> Articles can be viewed without a subscription.

[www.plantphysiol.org/cgi/doi/10.1104/pp.114.249003](http://www.plantphysiol.org/cgi/doi/10.1104/pp.114.249003)

wall CSC requires a minimum of three catalytic CESA proteins (Desprez et al., 2007; Persson et al., 2007).

On the basis of observations that cellulose microfibrils align with cortical microtubules (MTs) and that MT disruption leads to a loss of cell expansion, it was hypothesized that cortical MTs guide the deposition and, therefore, the orientation of cellulose (Green, 1962; Ledbetter and Porter, 1963; Baskin, 2001; Bichet et al., 2001; Sugimoto et al., 2003; Baskin et al., 2004; Wasteneys and Fujita, 2006). Confocal microscopy of CESA fluorescent fusions has advanced our understanding of CESA trafficking and dynamics. CSCs are visualized as small particles moving within the plane of the PM, with an average velocity of approximately 200 to 400 nm min<sup>-1</sup>. Their movement in linear tracks along cortical MTs (Paredes et al., 2006) supports the MT-cellulose alignment hypothesis.

Our current understanding of cellulose synthesis suggests that CESAs are assembled into CSCs in either the endoplasmic reticulum (ER) or the Golgi apparatus and trafficked by vesicles to the PM (Bashline et al., 2014; McFarlane et al., 2014). The presence of CESAs in isolated Golgi and vesicles from the trans-Golgi network (TGN) has been established by proteomic studies (Dunkley et al., 2006; Drakakaki et al., 2012; Nikolovski et al., 2012; Parsons et al., 2012; Groen et al., 2014). Their localization at the TGN has been corroborated by electron microscopy and colocalization with TGN markers, such as vacuolar H<sup>+</sup>-ATP synthase subunit a1 (VHA-a1), and the Soluble NSF Attachment Protein Receptor (SNARE) protein SYNTAXIN OF PLANTS41 (SYP41), SYP42, and SYP61 (Crowell et al., 2009; Gutierrez et al., 2009; Drakakaki et al., 2012). A population of post-Golgi compartments carrying CSCs, referred to as microtubule-associated cellulose synthase compartments (MASCs) or small cellulose synthase compartments (SmaCCs), may be associated with MTs or actin filaments and are thought to be directly involved in either CSC delivery to, or internalization from, the PM (Crowell et al., 2009; Gutierrez et al., 2009).

In addition to the CESAs, auxiliary proteins have been identified that play a vital role in the cellulose-synthesizing machinery. These include COBRA (Roudier et al., 2005), the endoglucanase KORRIGAN1 (KOR1; Lane et al., 2001; Lei et al., 2014b; Vain et al., 2014), and the recently identified POM-POM2/CELLULOSE SYNTHASE INTERACTIVE PROTEIN1 (POM2/CSI1; Gu et al., 2010; Bringmann et al., 2012). The latter protein functions as a linker between the cortical MTs and CSCs, as genetic lesions in POM2/CSI1 result in a lower incidence of coalignment between CSCs and cortical MTs (Bringmann et al., 2012). Given the highly regulated process of cellulose biosynthesis and deposition, it can be expected that many more accessory proteins participate in the delivery of CSCs and their interaction with MTs. Identification of these unique CSC-associated proteins can ultimately provide clues for the mechanisms behind cell growth and cell shape formation.

*Arabidopsis* (*Arabidopsis thaliana*) mutants with defects in the cellulose biosynthetic machinery exhibit a

loss of anisotropic growth, which results in organ swelling. This phenotype may be used as a diagnostic tool in genetic screens to identify cellulose biosynthetic and CSC auxiliary proteins (Mutwil et al., 2008). Chemical inhibitors complement genetic lesions to perturb, study, and control the cellular and physiological function of proteins (Drakakaki et al., 2009). A plethora of bioactive small molecules have been identified, and their analytical use contributes to our understanding of cellulose biosynthesis and CESA subcellular behavior (for review, see Brabham and Debolt, 2012). Small molecule treatment can induce distinct characteristic subcellular CESA patterns that can be broadly grouped into three categories (Brabham and Debolt, 2012). The first is characterized by the depletion of CESAs from the PM and their accumulation in cytosolic compartments, as observed for the herbicide isoxaben {*N*-[3-(1-ethyl-1-methylpropyl)-5-isoxazolyl]-2,6-dimethoxybenzamide}, CGA 325615 [1-cyclohexyl-5-(2,3,4,5,6-pentafluorophenoxy)-1,4,2,4,6-thiatriazin-3-amine], thaxtomin A (4-nitroindol-3-yl containing 2,5-dioxopiperazine), AE F150944 [N2-(1-ethyl-3-phenylpropyl)-6-(1-fluoro-1-methylethyl)-1,3,5-triazine-2,4-diamine], and quinoxiphen [4-(2-bromo-4,5-dimethoxyphenyl)-3,4-dihydro-1<sup>H</sup>-benzo-quinolin-2-one]; (Paredes et al., 2006; Bischoff et al., 2009; Crowell et al., 2009; Gutierrez et al., 2009; Harris et al., 2012). The second displays hyperaccumulation of CESAs at the PM, as seen for the herbicides dichlobenil (2,6-dichlorobenzonitrile) and indaziflam {*N*-[(1*R*,2*S*)-2,3-dihydro-2,6-dimethyl-1<sup>H</sup>-inden-1-yl]-6-(1-fluoroethyl)-1,3,5-triazine-2,4-diamine} (Herth, 1987; DeBolt et al., 2007b; Brabham et al., 2014). The third exhibits disturbance of both CESAs and MTs and alters CESA trajectories at the PM, as exemplified by morlin (7-ethoxy-4-methylchromen-2-one; DeBolt et al., 2007a). Unique compounds inducing a phenotype combining CESA accumulation in intermediate compartments and disruption of CSC-MT interactions can contribute to both the identification of the accessory proteins linking CSCs with MTs and the vesicular delivery mechanisms of CESAs.

In this study, we identified and characterized a unique cellulose deposition inhibitor, the small molecule CESA TRAFFICKING INHIBITOR (CESTRIN), which affects the localization pattern of CSCs and their interacting proteins in a unique way. The induction of cytoplasmic CESTRIN bodies might provide further clues for trafficking routes that carry CESAs to the PM.

## RESULTS

### CESTRIN Affects the Trafficking of CESA

Toward a better understanding of CSC trafficking, we screened a library of 360 small molecules of pollen germination and endosomal trafficking inhibitors (Drakakaki et al., 2011) for chemicals that specifically alter the localization of CESA in hypocotyls of 3-d-old etiolated *Arabidopsis* seedlings. We identified a compound, 1-[2,6-dinitro-4-(trifluoromethyl)phenyl]-2-[6-methyl-4-(trifluoromethyl)pyridin-2-yl]hydrazine,

$C_{14}H_9F_6N_5O_4$  (Supplemental Fig. S1), that induces distinct and pronounced changes in the localization pattern of CSCs in etiolated hypocotyls (Fig. 1). In control (i.e. dimethyl sulfoxide [DMSO]-treated) plants, GFP-CESA3 follows linear trajectories at the PM (Fig. 1A), as observed previously (Crowell et al., 2009; Gutierrez et al., 2009). Contrasting this, in the small molecule-treated plants, the overall presence of CSCs at the PM was substantially reduced. Furthermore, the particles showed reduced motility, as demonstrated in the translocation tracks of time-projected images (Fig.

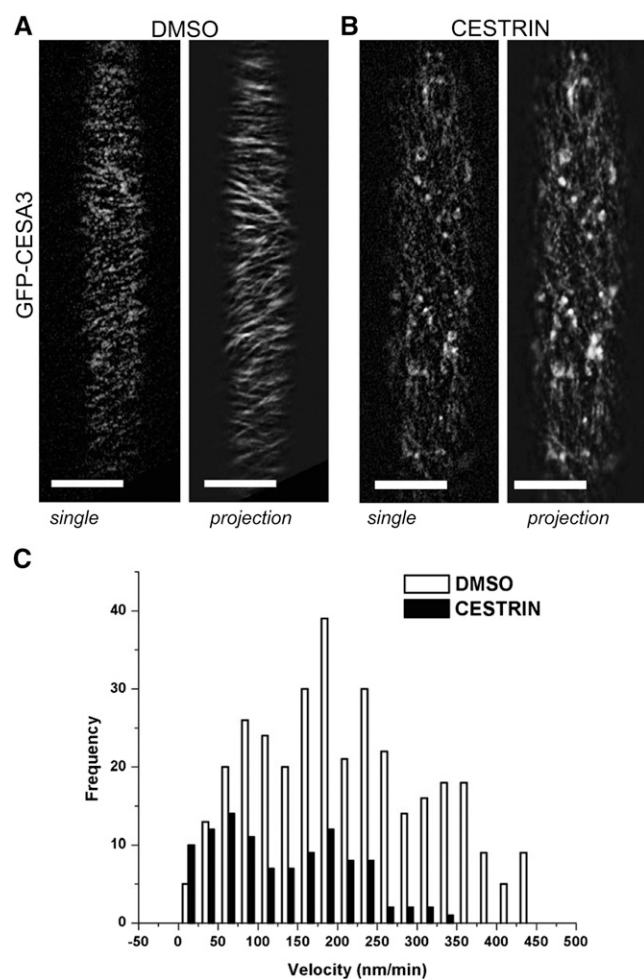


**Figure 1.** CESTRIN reduces GFP-CESA3 velocity (particle movement rate) and induces its accumulation in endomembrane compartments. Arabidopsis seedlings expressing GFP-CESA3 were grown in the dark for 3 d and imaged by spinning-disk confocal microscopy. A, Seedlings expressing GFP-CESA3 were treated with DMSO (control). A single optical section and, as an indication of motility, an average of 60 frames are shown. B, Upon a 2-h 15  $\mu$ M CESTRIN treatment, GFP-CESA3 particles no longer follow linear trajectories and are accumulated in punctae exhibiting increased fluorescence intensity. A single optical section and an average of 58 frames are shown. Bars in A and B = 10  $\mu$ m. C, Histogram showing the distribution of GFP-CESA3 velocities at the PM focal plane under DMSO (white bars;  $n = 349$ ) and CESTRIN (black bars;  $n = 105$ ) treatment.

1B). Analysis of time-lapse confocal imaging sequences revealed that the average velocity of the particles dropped from 218  $\text{nm min}^{-1}$  in the control plants to approximately 127  $\text{nm min}^{-1}$  in the treated ones (Fig. 1C; Supplemental Movies S1 and S2). Concurrently, much of the GFP-CESA3 accumulated in compartments at the cell cortex, exhibiting increased fluorescence intensity and larger size compared with the control. It is likely that this subcellular population contains the CSCs in SmaCCs/MASCs (Crowell et al., 2009; Gutierrez et al., 2009). Given the effect on CESA trafficking, we refer to the compound as CESTRIN and to the cytoplasmic compartments as CESTRIN-induced bodies.

In order to assess the specificity of CESTRIN, a variety of organelle markers and their subcellular localizations were examined in Arabidopsis etiolated hypocotyls. The unaltered morphology of endosomes labeled by CLATHRIN LIGHT CHAIN2 (CLC2)-GFP demonstrates that CESTRIN does not target endocytic trafficking (Fig. 2A). Furthermore, the localization of neither secretion marker sec-GFP nor the PM-receptor-like kinase THESEUS1 (THE1)-GFP was altered (Fig. 2, B and C), suggesting that the drug does not broadly disrupt trafficking to the PM or secretion. The overall morphology of the ER, Golgi, TGN, early endosomes, and vacuole and the trafficking of soluble cargo to the vacuole were not noticeably affected (Supplemental Fig. S2), indicating that

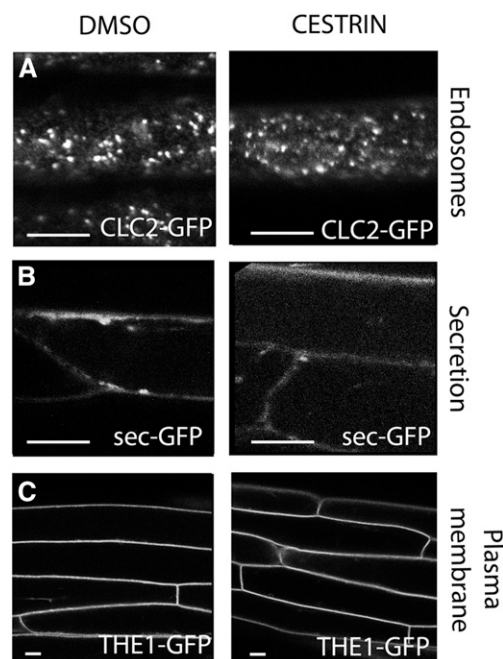


**Figure 2.** CESTRIN does not broadly disrupt trafficking to the PM or secretion in Arabidopsis hypocotyls. Three-day-old etiolated Arabidopsis seedling hypocotyls were observed in the confocal microscope for either DMSO or 2-h CESTRIN treatment. Seedlings expressing CLC2-GFP (A), sec-GFP, a secretion marker (B), and THE1-GFP, a PM receptor-like kinase (C), did not show localization or morphological defects after CESTRIN treatment. Bars = 10  $\mu$ m.

CESTRIN does not exert broad toxicological effects in *Arabidopsis* etiolated hypocotyls. Taken together, these results suggest that CESTRIN perturbs the localization and motility of compartments involved in CSC trafficking. Evaluating if CESTRIN causes a broad growth inhibition, we analyzed its impact on bacteria (*Escherichia coli*), for which no effect on their proliferation was observed ( $P = 0.89$  at  $7 \mu\text{M}$ ; Supplemental Fig. S3A); however, minor growth defects were observed for yeast (*Saccharomyces cerevisiae*; Supplemental Fig. S3B).

### CESTRIN Inhibits Cell Elongation and Reduces Cellulose Content

CESTRIN reduced anisotropic cell growth in a concentration-dependent manner, with an estimated half-maximal inhibitory concentration of  $4.85 \mu\text{M}$  (Fig. 3, A and B) in 5-d-old etiolated seedlings germinated on CESTRIN-containing medium. CESTRIN induced changes in hypocotyl cell morphology, with clearly visible cell swelling and reduced cell elongation (Fig. 3, C and D). CESTRIN also impacted cellulose production: *Arabidopsis* hypocotyls grown on  $9 \mu\text{M}$  CESTRIN contained approximately 30% less cellulose compared with control seedlings (Table I). To assess the short-

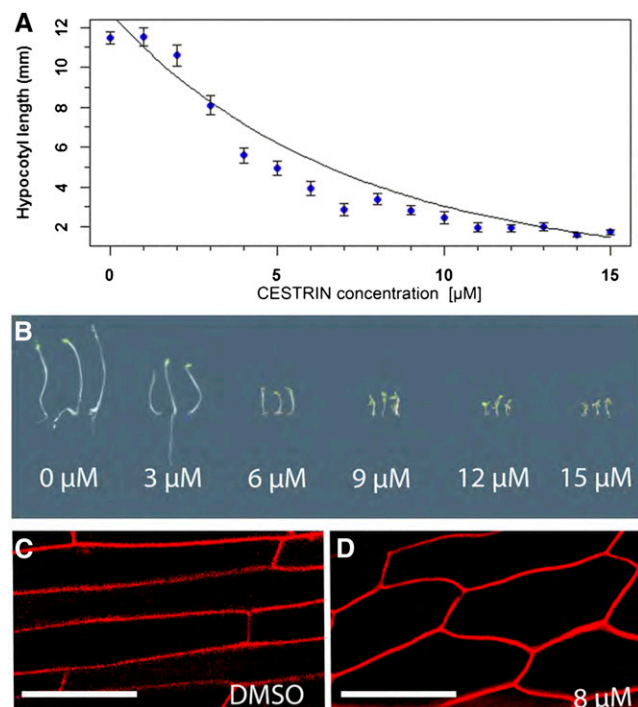


**Figure 3.** CESTRIN inhibits anisotropic growth in *Arabidopsis*. A and B, Concentration-dependent growth inhibition of 5-d-old *Arabidopsis* etiolated hypocotyls under CESTRIN treatment. The half-maximal inhibitory concentration is calculated to be  $4.85 \mu\text{M}$  using an exponential trend line ( $r^2 = 0.9416$ ,  $n = 48$ ). C and D, Propidium iodide staining of hypocotyl cells in 5-d-old *Arabidopsis* seedlings treated with CESTRIN shows decreased elongation and increased radial swelling. Bars =  $50 \mu\text{m}$ .

**Table I.** CESTRIN treatment significantly reduces cellulose content in *Arabidopsis* etiolated seedlings

Cellulose content is shown in  $\mu\text{g mg}^{-1}$  of alcohol-insoluble residues (AIR). The asterisk indicates a significant difference in cellulose content as measured in dark-grown hypocotyls ( $P < 0.01$  by Student's *t* test).

Treatment	Cellulose Content
DMSO	$103.7 \pm 6.4$
CESTRIN ( $9 \mu\text{M}$ )	$75.3 \pm 2.7^*$

term effects of CESTRIN on Glc incorporation, we performed a 2-h pulse chase on 3-d-old etiolated seedlings using  $[^{13}\text{C}]\text{Glc}$ . We monitored the relative incorporation of  $^{13}\text{C}$  into the Glc detected in the cellulose fraction, using gas chromatography-mass spectrometry analysis of alditol acetates generated after hydrolysis of the cellulose fraction. Selective ion monitoring mode, as described previously (Greve and Labavitch, 1991; Huysamer et al., 1997), indicated that CESTRIN significantly decreased the amount of  $[^{13}\text{C}]\text{Glc}$  that was incorporated into the cellulose fraction; this reduction was greater when more CESTRIN was applied ( $P < 0.00001$  for  $15 \mu\text{M}$ ,  $P = 0.000124$  for  $8 \mu\text{M}$ ) in our short-term treatment (Table II). In addition, a less profound but still significant reduction was observed in the 2 N trifluoroacetic acid (TFA)-hydrolyzed cell wall fraction (i.e. the noncellulosic neutral sugars) of the isolated cell walls ( $P = 0.0176$  for  $15 \mu\text{M}$ ,  $P = 0.0325$  for  $8 \mu\text{M}$ ), suggesting reduced incorporation of  $[^{13}\text{C}]\text{Glc}$  into structural polysaccharides.

### CESTRIN Treatment Induces Mislocalization of the CESA-Interacting Proteins POM2/CSI1 and KOR1

Recent studies have shown that the glucanase KOR1 is an integral part of the primary cell wall CSCs at the PM (Vain et al., 2014). Similar to CSCs, the localization pattern of KOR1 follows MT reorientation during epidermal cell elongation (Lei et al., 2014b; Vain et al., 2014). We investigated if CESTRIN affects CESAs or KOR1 in a differential manner by comparing the respective localization patterns. Under control conditions, GFP-KOR1-labeled PM particles migrate along linear trajectories with comparable velocities (average of  $220 \text{ nm min}^{-1}$ ) to those observed for GFP-CESAs (Fig. 4, A and C). Overall, the trafficking pattern of CSCs and KOR1 showed similar behavior after CESTRIN treatment; however, subtle differences also were evident. CESTRIN treatment dramatically reduced the presence of mobile, PM-localized GFP-KOR1 and instead concentrated the protein in trafficking compartments at the cell cortex, as judged from the higher fluorescence intensity (Fig. 4, B and C). The mean velocity of GFP-KOR1-labeled particles was reduced to approximately  $60 \text{ nm min}^{-1}$  (Fig. 4C), with particle motion resembling a random walk rather than following straight trajectories.

CESAs involved in primary cell wall biosynthesis interact with POM2/CSI1 (Gu et al., 2010; Bringmann et al., 2012), which prompted an investigation into the

**Table II.** [<sup>13</sup>C]Glc incorporation into cellulose under CESTRIN treatment

Values shown are [<sup>13</sup>C]Glc:[<sup>12</sup>C]Glc × 100. Asterisks indicate significant differences in [<sup>13</sup>C]Glc incorporation under 2-h treatment in dark-grown Arabidopsis seedlings (\*\**P* < 0.01; \*0.01 < *P* < 0.05 by Student's *t* test).

Treatment	Cellulose Fraction	Soluble Fraction
DMSO	2.37 ± 0.01	4.16 ± 1.1
CESTRIN (15 μM)	0.44 ± 0.01**	1.65 ± 1.87*
CESTRIN (8 μM)	0.76 ± 0.19**	1.97 ± 0.43*

trafficking dynamics of POM2/CSI1 fused with triple yellow fluorescent protein for energy transfer Ypet (3xYpet) under CESTRIN treatment. In control plants, the localization pattern of POM2/CSI1-3xYpet showed distinct punctae that exhibit a directional motility (Fig. 4D), in accordance with previous observations (Gu et al., 2010; Bringmann et al., 2012). However, in CESTRIN-treated plants, POM2/CSI1-3xYpet-labeled particles lost organization, leading to a more dispersed localization (Fig. 4E). This behavior occurred concurrent with the reduction in directional movement after approximately 1.5 h of CESTRIN treatment (Fig. 4E). After 2 h of treatment, we observed a diffuse, cytoplasmic pattern of the fluorescent signal, suggesting that the POM2/CSI1 became disengaged from the PM CSCs. The average motility of POM2/CSI1-labeled particles was reduced from approximately 262 to 164 nm min<sup>-1</sup> after about 1.5 h of treatment (Fig. 4F). Overall, these data suggest that CESTRIN inhibits the dynamics of CSCs, KOR1, and POM2/CSI1 and alters a cellulose-related pathway.

### CESTRIN Alters MT Stability in a Mechanism Different from Oryzalin

Given that CESAs interact closely with MTs, we studied the effect of CESTRIN on MT stability and organization using Arabidopsis seedlings expressing GFP-CESA3/mCherry-TUA5 (for red monomeric fluorescent protein attached to tubulin α-5; Gutierrez et al., 2009). Concurrent with the pronounced mislocalization of GFP-CESA3, CESTRIN treatment induced marked changes in MT organization, including a reduction in transverse-oriented cortical arrays in comparison with DMSO-treated controls (Fig. 5). The majority of the treated cells featured disordered MT arrays or more diffuse fluorescence patterns (Fig. 5; Supplemental Fig. S4A). To further investigate the impacts of CESTRIN on MT arrays, we examined the localization pattern of the MT plus-end binding protein END BINDING1 (EB1; Chan et al., 2003; Dixit et al., 2006). As described previously, GFP-EB1 localizes in distinct foci that dominantly label MT plus ends (Supplemental Fig. S4B). In contrast, CESTRIN-treated cells showed diffuse EB1 fluorescence in the cytoplasm (Supplemental Fig. S4B). It is likely that the loss of MT stability due to CESTRIN treatment leads to the loss of MT-localized EB1. Additionally, despite these MT behavioral effects under CESTRIN treatment, the MT tip disconnection from the

cortex (Shaw et al., 2003) is not increased (*P* = 0.19; Supplemental Movies S3 and S4).

Under normal conditions, CESAs are typically delivered to sites that coincide with cortical MTs (Gutierrez et al., 2009). A possible explanation for the observed CESA behavior under CESTRIN treatment could be a failure to deliver CESAs to MT sites and/or an inability to properly guide the CSCs along the MTs. This hypothesis in turn prompted us to compare CESTRIN with the MT depolymerization drug oryzalin, which binds tubulin dimers and interferes with the dimer addition to MT ends (Morejohn et al., 1987). The effect of CESTRIN on cortical MT array organization shares partial similarities with oryzalin. As mentioned above, CESTRIN treatment caused alterations in the organization and depolymerization of MTs, leading to less defined arrays and a more diffuse pattern of presumably free mCherry-TUA5 (Fig. 5B; Supplemental Fig. S4A). This effect is similar for oryzalin, although less pronounced under CESTRIN treatment. A dramatically different behavior was observed for the cellular dynamics of CSCs during treatment with CESTRIN than that with oryzalin. Even under extended oryzalin treatment, the CSCs do not dissociate from the PM, unlike the phenotype observed under CESTRIN treatments (Supplemental Fig. S4A; Paredez et al., 2006; Gutierrez et al., 2009). To further investigate if CESTRIN is a direct MT polymerization inhibitor, we employed an *in vitro* spectrometric absorption assay. The assay did not yield any evidence for CESTRIN inhibiting the tubulin polymerization process *in vitro*; there was, however, a slight but significant increase in polymerization (*P* = 0.011; Supplemental Fig. S4D).

In stark contrast to the distinct changes in the MT, no changes were observed for actin organization and dynamics under chemical treatment (Supplemental Fig. S4C), which further demonstrates that the small molecule does not broadly affect the cytoskeleton.

### CSCs Are Enriched in SYP61-Associated Compartments upon CESTRIN Treatment

The apparent redistribution of CSCs from the PM to the cell cortex prompted us to further investigate the identity of the CESTRIN bodies. Previous studies have shown that CSCs are partially colocalized with SYP61/VHA-a1 in early endosome/TGN compartments (Crowell et al., 2009; Gutierrez et al., 2009). The presence of CESAs in SYP61 vesicles was further established by proteomic analysis (Drakakaki et al., 2012). Moreover, of several endosomal/TGN markers investigated previously, SYP61 was shown to partially overlap with cortically tethered SmaCCs (Gutierrez et al., 2009). As shown previously, both SYP61 and SYP41/42 partially overlap with CESA6 under mock treatment; however, only SYP61 remains partially colocalized with the CESA signal after mannitol treatment (Gutierrez et al., 2009). Therefore, we examined the behavior of GFP-CESA3 in relationship to SYP61 under CESTRIN treatment. Partial colocalization of the GFP-CESA3 and cyan fluorescent protein (CFP)-SYP61

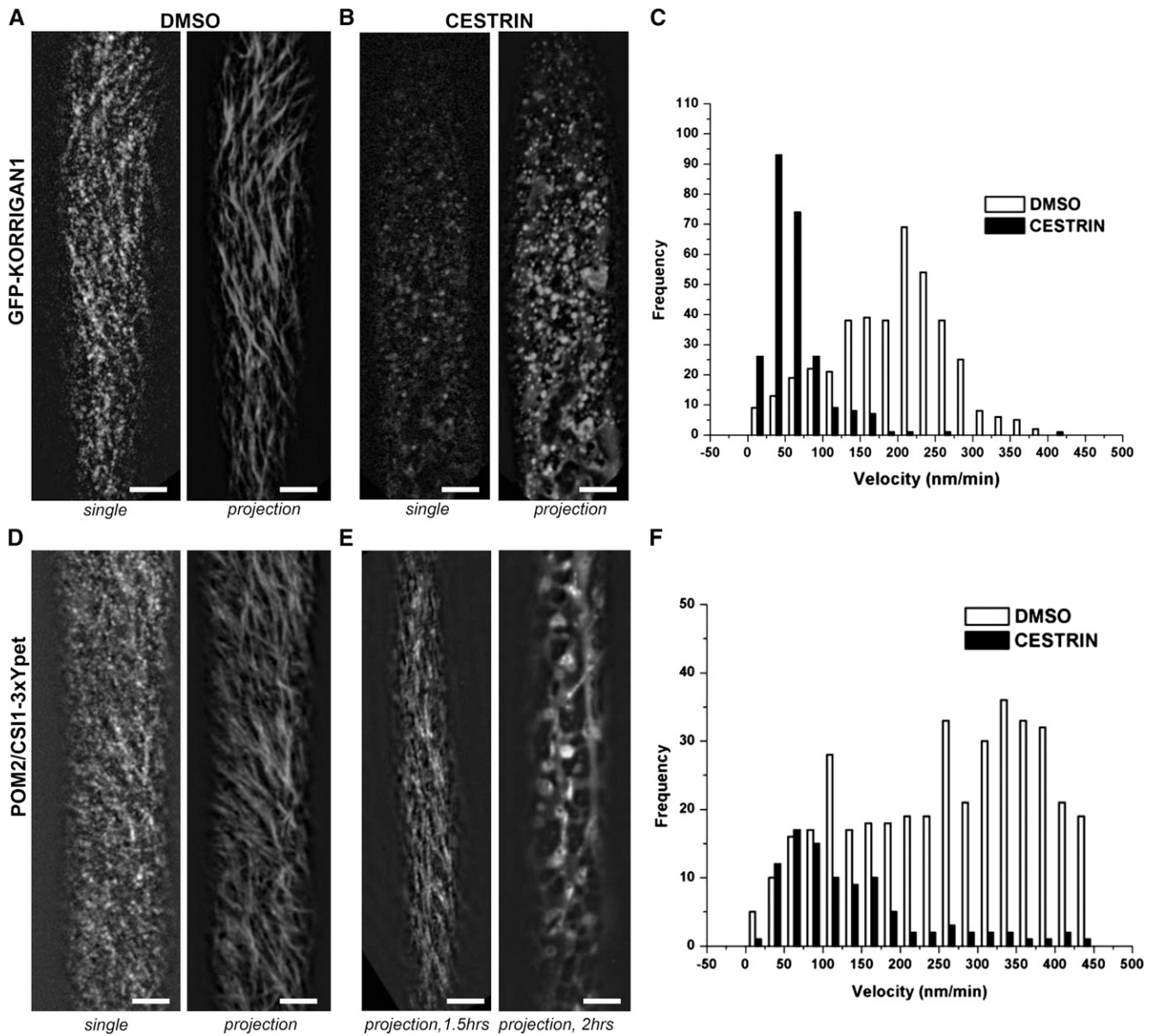


**Figure 4.** CESTRIN alters the localization and velocity of GFP-KOR1 and POM2/CSI1-3xYpet. Arabidopsis seedlings expressing GFP-KOR1 and POM2/CSI1-3xYpet were grown in the dark for 3 d and imaged by spinning-disk confocal microscopy. A, Seedlings expressing GFP-KOR1 were treated with DMSO (control). A single optical section and an average of 50 frames are shown. B, Upon a 2-h 15 μM CESTRIN treatment, GFP-KOR1 particles are accumulated in punctae exhibiting increased fluorescence intensity. A single optical section and an average of 55 frames are shown. Bars in A and B = 5 μm. C, Histogram showing the frequency of GFP-KOR1 velocities at the PM focal plane under DMSO (white bars; n = 406) or 15 μM CESTRIN (black bars; n = 247) treatment. D, Seedlings expressing POM2/CSI1-3xYpet were treated with DMSO (control). A single optical section and an average of 58 frames are shown. E, Upon a 1.5-h 15 μM CESTRIN treatment, POM2/CSI1-3xYpet particles show an altered distribution pattern, as shown by a 60-frame average. Upon a 2-h 15 μM CESTRIN treatment, POM2/CSI1-3xYpet was localized to the cytoplasm; an average of 60 frames is shown. Bars in D and E = 5 μm. F, Histogram showing the frequency of POM2/CSI1-3xYpet velocities at the PM focal plane under DMSO (white bars; n = 420) or 15 μM CESTRIN (black bars; n = 106) treatment.

compartments was observed under DMSO treatment and was enhanced significantly (approximately 15%) upon CESTRIN application ( $P = 0.0013$ , Student's  $t$  test; Fig. 6). Our data corroborate the presence of CSCs in SYP61 vesicles, which is increased by CESTRIN treatment.

#### Isoxaben-Resistant Plants Are Not Resistant to CESTRIN

To determine if CESTRIN acts on the CESAs in a similar manner to that of the well-characterized cellulose inhibitor isoxaben, we compared the hypocotyl growth in etiolated seedlings of the isoxaben-resistant

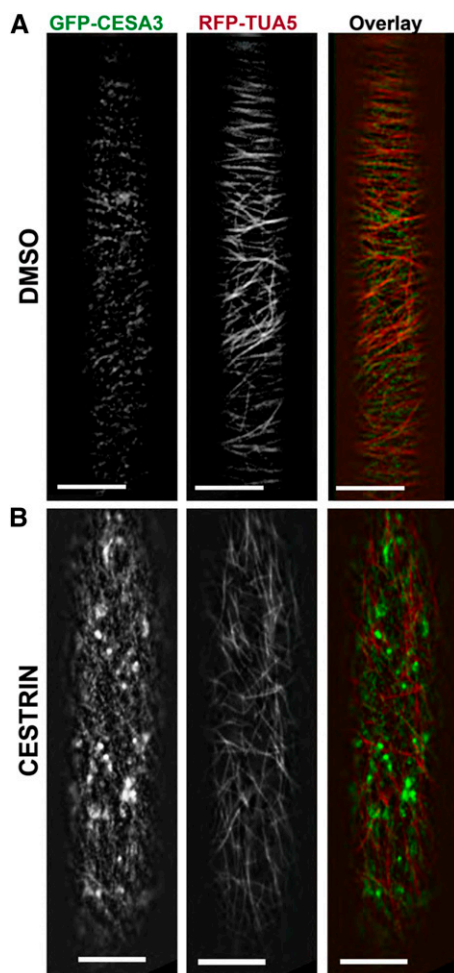


**Figure 5.** CESTRIN alters MT organization concurrent with GFP-CESA3 mislocalization. Three-day-old etiolated *Arabidopsis* seedlings expressing both RFP-TUA5 and GFP-CESA3 were imaged. A, DMSO-treated seedlings. A trace from six frames shows colocalization of GFP-CESA3 particles and MTs. B, A 2-h 15  $\mu\text{M}$  CESTRIN treatment causes loss of MT organization and redistribution of GFP-CESA3 particles. The trace was composed of 58 frames. Bars = 10  $\mu\text{m}$ .

*CESA3* mutant *ixr1-1* (Heim et al., 1989; Scheible et al., 2001) with that of wild-type Columbia (Col-0) and the *CESA6*, *procuste1* (*prc1-1*) allele (Fagard et al., 2000). While the hypocotyl growth of *ixr1-1* was resistant to isoxaben treatment ( $P = 0.2$ ), a 62% reduction in elongation was observed when the mutant was grown on CESTRIN-containing plates ( $P = 8.6 \times 10^{-5}$ ). However, the reduction was more pronounced for the wild-type Col-0, exhibiting an 80% reduction ( $P = 0.001$ ; Fig. 7). When comparing Col-0 and *ixr1-1*, the two genotypes showed significantly different responses to the two chemicals (two-way ANOVA,  $P = 4.7 \times 10^{-12}$ ). In addition, a significantly different response of *prc1-1* compared with Col-0 was observed for both chemical treatments (two-way ANOVA,  $P = 0.008$ ). The *prc1-1* mutant showed sensitivity to both isoxaben and CESTRIN, although to a

lower degree compared with the growth reduction in the wild-type Col-0. Taken together, these data indicate that isoxaben and CESTRIN have distinct targets or mechanisms of action.

## DISCUSSION

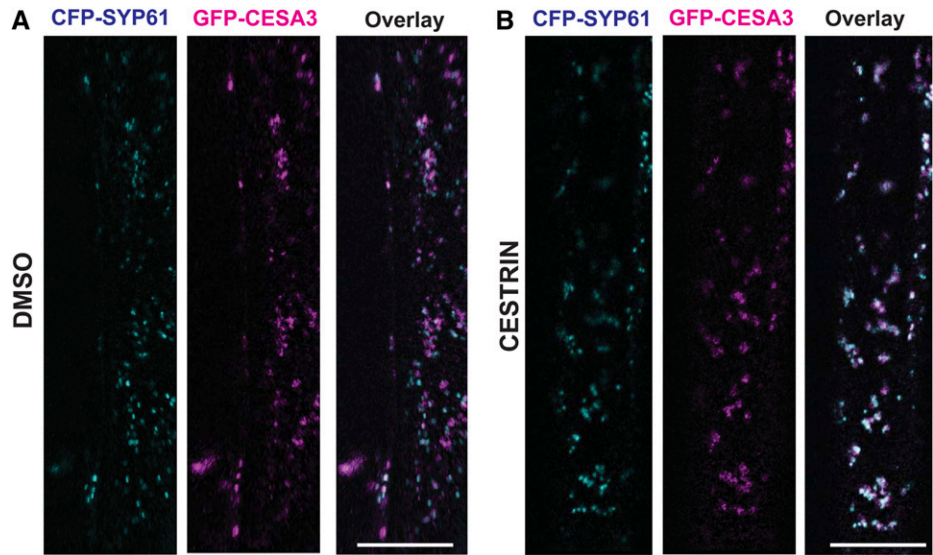
Although recent studies have identified a molecular component that mediates the interaction between CESAs and MTs, many unknown players potentially await discovery. In addition, the cellular determinants that control CSC delivery to, and internalization from, the PM remain ill understood (Lei et al., 2014a; McFarlane et al., 2014). Such unique components could be critical for regulating the stability and activity of CSCs and may reveal new aspects of anisotropic cell growth. We have identified a compound, CESTRIN, that alters the trafficking of CSCs and their associated proteins POM2/CSI1 and KOR1, leading to MT instability and a reduction in cellulose content.

CESTRIN did not affect the localization patterns of a variety of endomembrane compartments, including the ER, Golgi, TGN, and vacuole, demonstrating that the subcellular phenotype is not the result of broad cell toxicity. Strikingly, neither general secretion nor cytosolic clathrin compartments were affected, indicating that CESTRIN's mode of action does not indiscriminately affect endocytic or secretion pathways but rather selective pathways involved in CESA delivery in *Arabidopsis* etiolated hypocotyls.

Exposure to CESTRIN increased the colocalization of SYP61 vesicles with CESA, suggesting that CESTRIN bodies are enriched in the syntaxin. Mannitol treatment is thought to tether MT to SmaCCs. Corroborating our findings, mannitol-induced SmaCCs only colocalized partially with SYP61 among the different TGN markers tested (Gutierrez et al., 2009). Moreover, proteomic analysis of SYP61 vesicles has established that they contain CESAs involved in primary cell wall biosynthesis and KOR1 (Drakakaki et al., 2012), suggesting a role of SYP61 in the trafficking of CSCs. A recent TGN proteomic analysis identified CESA1 in VHA-a1 fractions; however, neither CESA3/6 nor KOR1 could be detected (Groen et al., 2014). A plausible explanation might be that SYP61 defines a population that is distinct from VHA-a1 vesicles involved in the delivery of CSCs, although other currently uncharacterized populations may be involved as well.

Our studies showed that the two CESA-interacting proteins POM2/CSI1 and KOR1 are affected by CESTRIN; however, subtly different behaviors were observed for the two. The nature of these proteins might give clues about their subcellular behavior after CESTRIN treatment. POM2/CSI1 is currently the most well-characterized protein that serves as a linker between MT and CSCs. In vitro assays demonstrated that it interacts both with MTs and CESAs involved in primary cell wall synthesis, while in planta studies have shown that it colocalizes with CESAs while traveling along trajectories aligned with MT CSCs (Gu et al.,

**Figure 6.** CESTRIN causes an increase in colocalization between CSCs and SYP61 in *Arabidopsis* hypocotyls. Colocalization of CFP-SYP61 (magenta) and GFP-CESA3 (cyan) in etiolated *Arabidopsis* hypocotyls (A) increases under 2 h of 15  $\mu\text{M}$  CESTRIN treatment when compared with the DMSO control (B). A 15% increase in the colocalization of GFP-CESA3 and CFP-SYP61 particles was observed. Analysis was performed on three time series per treatment, acquired by sequential line scanning. Bars = 10  $\mu\text{m}$ .



2010; Bringmann et al., 2012; Li et al., 2012). In addition, genetic lesions in *pom2/csi1* null mutants exhibit both CSCs and cortical MT defects (Bringmann et al., 2012; Li et al., 2012; Mei et al., 2012; Landrein et al., 2013).

The glucanase KOR1 interacts with CESAs involved in primary cell wall formation and colocalizes with CESAs at the PM moving along linear trajectories. Moreover, KOR1-GFP is present in SmaCCs/MASCs and at the Golgi, TGN, and late endosome compartments (Robert et al., 2005; Lei et al., 2014b; Vain et al., 2014). Under CESTRIN treatment, KOR1-GFP displays subcellular patterns similar to that of GFP-CESA3; both localize in bright fluorescent punctae. This observation suggests that the membrane association of CESAs and KOR1 is maintained upon chemical treatment, leading to their enhanced localization in the intermediate

CESTRIN bodies. This is in contrast to the partial cytoplasmic localization of POM2/CSI1 upon chemical treatment, which suggests a dissociation from CSCs. The fact that CESTRIN targets both proteins associated with CSCs underscores the selectivity of CESTRIN toward a pathway potentially controlling the interaction between the two.

Cellulose biosynthesis inhibitors (CBIs) influence the trafficking and dynamics of CESAs or MTs (Brabham and Debolt, 2012; McFarlane et al., 2014). Small molecules such as isoxaben, CGA 325615, and mannitol deplete CSCs from the PM, leading to their subsequent accumulation in SmaCCs/MASCs (Crowell et al., 2009; Gutierrez et al., 2009). CESTRIN is unique in causing CSC accumulation in CESTRIN bodies while concurrently affecting MT organization. The way CESTRIN influences

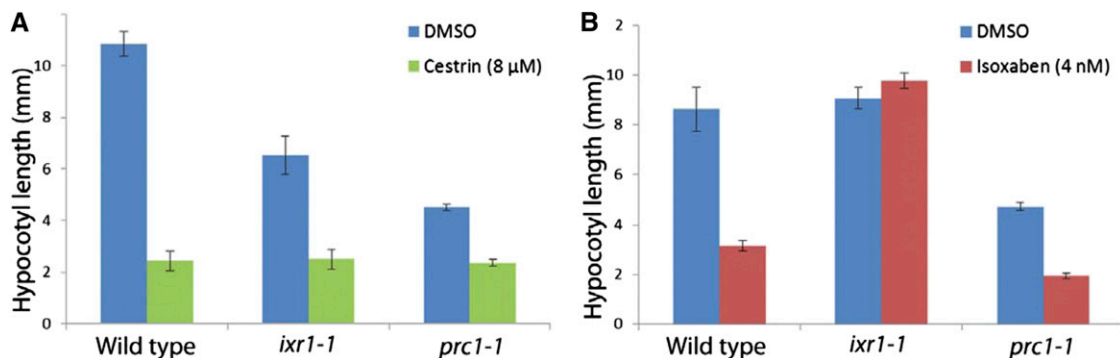


**Figure 7.** The isoxaben-resistant mutant *ixr1-1* did not display cross resistance to CESTRIN. A, Hypocotyl growth of wild-type Col-0, the isoxaben-resistant CESA3 mutant *ixr1-1*, and the CESA6 mutant *prc1-1* in 8  $\mu\text{M}$  CESTRIN compared with DMSO-supplemented medium ( $n = 16$  seedlings per treatment). B, Wild-type Col-0, *ixr1-1*, and *prc1-1* 5-d-old seedlings were grown on medium containing 4 nM isoxaben or DMSO ( $n = 16$  seedlings per treatment). The hypocotyl growth of *ixr1-1* was reduced under CESTRIN treatment by 62% ( $P = 8.6 \times 10^{-5}$ ), while it was not reduced under isoxaben treatment ( $P = 0.2$ ) when compared with wild-type Col-0. When comparing Col-0 and *ixr1-1*, the two genotypes showed significantly different responses to the two chemicals (two-way ANOVA,  $P = 4.7 \times 10^{-12}$ ). Significantly different responses of *prc1-1* compared with Col-0 were observed for both chemical treatments (two-way ANOVA,  $P = 0.008$ ).

the stability of MTs is markedly different from that observed for CBIs and oryzalin. Application of oryzalin at a concentration depolymerizing MTs has no significant effect on the velocity and localization of CSCs (DeBolt et al., 2007a); however, extended oryzalin treatment results in a complete removal of MTs and a uniform distribution of CSCs at the PM (Gardiner et al., 2003; Li et al., 2012). Furthermore, under MT depolymerization conditions, no dissociation of POM2/CSI1 with CSCs is observed, despite their localization in less-defined trajectories (Bringmann et al., 2012). The only previously described effect of oryzalin on CSC trafficking is in combination with other CBIs (Gutierrez et al., 2009; Sampathkumar et al., 2013). In contrast to oryzalin, which inhibits tubulin polymerization *in vitro* at a concentration of 5  $\mu\text{M}$  (Morejohn et al., 1987), CESTRIN application at a concentration inducing CESTRIN bodies (15  $\mu\text{M}$ ) does not inhibit *in vitro* tubulin polymerization. This suggests that MT instability and depolymerization are not likely the primary effects of the small molecule but possibly a feedback mechanism, through an intermediate component associating with both CESAs and MT. For example, those could include POM2/CSI1 or other not-yet identified proteins involved in this interaction. Null mutants of *pom2/csi1* have decreased elongation and increased swelling in hypocotyls, reduced velocity of CSCs, reduced cellulose content, and disorganized MTs, which are phenocopied by CESTRIN application (Bringmann et al., 2012; Gu et al., 2010).

The CBIs morlin and cobtorin (4-[(2-chlorophenyl)methoxy]-1-ntirobenzene) affect cytoskeleton organization but do not cause CSC accumulation in intermediate bodies (DeBolt et al., 2007a; Yoneda et al., 2007, 2010). The distinct subcellular phenotypes caused by CESTRIN compared with oryzalin, morlin, and cobtorin illustrate that CESTRIN has a markedly different mode of action, featuring an altered trafficking of extended CSCs and causing their accumulation in intermediate CESTRIN-induced bodies while affecting the MT-CSC interaction.

Further corroborating that CESTRIN affects cellulose deposition is the fact that seedlings grown in the presence of the compound display an approximately 30% reduction in cellulose, with additional reduction in [ $^{13}\text{C}$ ] Glc in the 2 N TFA-insoluble cell wall fraction after 2 h of CESTRIN treatment. In addition, our data show that CESTRIN does not act on MT polymerization directly under our *in vitro* conditions, and the MT phenotype observed may be due to feedback from CSC disruption. The notion of feedback disruption from cell wall to cytoskeleton organization is supported by genetic studies in which it was shown that mutations in the genes encoding the glucanase KOR1 and CESA6 (*kor1-3*, *prc1-20*, and *jiayao1*) resulted in changes of MT organization (Paredes et al., 2008; Lei et al., 2014b). It is plausible that CESTRIN's inhibition of the CSCs provides feedback to the MT, which in turn leads to a disorganized or collapsing MT array. However, we cannot rule out the possibility that CESTRIN may be acting upon MTs *in vivo*, changing their behavior by mechanisms other than direct polymerization but perhaps interfering with

additional factors, which could lead to altered trafficking of CESA. It is possible that the small molecule acts on a linker protein between CSCs and MTs, such as the POM2/CSI1 or other not-yet identified proteins involved in this interaction.

Despite the reduction in cellulose content, we reason that CESTRIN affects CESA, employing a different mode of action than observed for isoxaben. The sensitivity of the *ixr1-1* mutant to CESTRIN, in contrast to that of isoxaben resistance, implies that even if a CESA subunit is targeted by CESTRIN, it does not correspond to the *ixr1-1* locus on CESA3. A number of mechanisms can account for the cumulative observed behavior of CESTRIN, although it is challenging to ascribe likelihoods to these mechanisms with certainty. We put forward some plausible hypotheses.

CESTRIN might affect a signaling mechanism regulating the activity of CSCs, potentially mediated by phosphorylation. It is known that changes in CESA phosphorylation alter their motility and reduce anisotropic growth (Chen et al., 2010; Bischoff et al., 2011). Further interactions of MT-associated proteins and MTs can be modulated via phosphorylation by altering protein surface charge (Smertenko et al., 2006, 2008). Hence, it is tempting to suggest that CESTRIN targets phosphorylation; however, on the basis of the observed reduction in cellulose content and the formation of CESTRIN bodies, without affecting MT polymerization *in vitro*, this seems unlikely. Another possible mechanism is that signaling events may take place that cause the accumulation of CSCs to CESTRIN bodies and feedback, altering MT stability. It is also possible that CESTRIN affects substrate availability during the biosynthesis of cellulosic glucans and cell wall polysaccharides. This effect could take place during the nucleotide sugar conversion pathway. Detailed analysis of monosaccharides in the matrix polysaccharide fraction is under way to examine the effects of CESTRIN in the overall UDP-Glc conversion and utilization. Only future studies that identify the target of CESTRIN and identify the mode of action of CESTRIN can conclusively determine which of these hypotheses is correct; these efforts are currently under way.

Our study has identified CESTRIN, a unique inhibitor of processes associated with cellulose deposition that alters the trafficking of CSCs and their interacting proteins, enriching the CSC population in SYP61 compartments. CESTRIN affords unique avenues to study and understand the mechanism under which PM-associated CSCs are maintained and interact with MTs and to dissect trafficking routes that deliver CSCs to the PM.

## MATERIALS AND METHODS

### Plant Materials and Growth for Microscopy Studies

*Arabidopsis* (*Arabidopsis thaliana*) seeds were sterilized using 30% (v/v) sodium chlorate in ethanol (absolute) with 30  $\mu\text{L}$  of Triton X-100 (Sigma) per 50 mL of solution. Seeds were plated on 0.5 $\times$  *Arabidopsis* growth medium (AGM) with phytagar (2.3 g L $^{-1}$  Murashige and Skoog [MS] minimal organics medium, 10 g L $^{-1}$  Suc, and 8 g L $^{-1}$  phytagar) and cold vernalized for 48 h at 4°C in the dark. Plates were transferred to a 24°C growth chamber, exposed upright

to light for 3 h, and etiolated in the dark for 3 d prior to chemical treatment and further examination.

After 3 d, seedlings were transferred to 24-well plates containing 0.8 mL of 0.5× AGM with phytagar supplemented with 0.5% (v/v) DMSO (Sigma), 15 μM CESTRIN (12 mM stock), or 30 μM oryzalin (40 mM stock; Fisher 50-748-30). To ensure consistency, all treatments were carried out in phytagar-supplemented medium. Pulse treatments of Arabidopsis seedlings with the desired chemicals were performed for 2 h in the dark.

Transgenic lines expressing MANNOSIDASE-yellow fluorescent protein (MAN-YFP; Nebenführ et al., 1999); the ER marker HDEL-GFP (Nelson et al., 2007); the vacuolar marker, vesicle-associated membrane protein711 (VAMP711-YFP; Geldner et al., 2009); the vacuolar marker containing the N-terminal vacuolar sorting signal fused to red fluorescent protein (NTPppro-RFP; Hunter et al., 2007); the THE1-GFP (Hématy et al., 2007), the CLC2-GFP (Konopka et al., 2008), the endosomal/TGN marker VHA-a1-RFP (Dettmer et al., 2006); the endosomal/TGN marker vesicle transport V-SNARE12 (VTI12-YFP; Geldner et al., 2009); the endosomal/TGN marker syntaxin of plants61 fused to CFP (CFP-SYP61; Robert et al., 2008), the sec-GFP (Zheng et al., 2004), the cellulose synthases CESA6-YFP (Paredes et al., 2006) and GFP-CESA3 (Desprez et al., 2007); the double cellulose synthase/tubulin marker GFP-CESA3/mCherry-TUA5 (Gutiérrez et al., 2009); the tubulin marker TUB-GFP (Nakamura et al., 2004), the EB1-GFP (Dixit et al., 2006), and the actin marker TALIN-GFP (Mathur et al., 1999) were used.

## Plant Expression Vectors

POM2/CSII-3xYpet was created using the basic experimental procedures described by Zhou et al. (2011) by employing the transformation competent artificial clone JAtY77F05 to generate an in-frame C-terminal translational fusion between the CSII/POM2 gene (AT2G22125) and the 3xYpet tag (Arabidopsis Biological Resource Center stock no. CD3-1727). All of the Arabidopsis genomic sequences in the clone JAtY77F05 10 kb upstream and 5 kb downstream of POM2/CSII were replaced by recombineering using the ampicillin and tetracycline resistance genes, respectively. Primers used in this procedure and verification of insertion are shown in Supplemental Table S1. The resulting plasmid was transformed into plants using *Agrobacterium tumefaciens* strain GV3101 standard protocols. T2 transformants were selected by BASTA (glufosinate ammonium; 200 g L<sup>-1</sup>) spray, and gene expression was validated by confocal microscopy.

## Microscopy and Image Analysis

Spinning-disk confocal microscopy to observe the dynamics of CESA3-GFP × TUA5-RFP, POM2-3xYpet, and KOR1-GFP (Vain et al., 2014) was performed using two similar customized microscopes (3I) equipped with spinning-disk heads (Yokogawa), electron-multiplying charge-coupled device cameras (Andor and Photometrics), and oil-immersion objectives (100×, numerical aperture 1.4). Time-lapse images were taken every 5 s, with exposure times between 600 and 800 ms.

Confocal images for CFP-SYP61 × CESA3-GFP were obtained using a Leica SP5 microscope using a 63× water objective employing dual-channel sequential line scanning. Fluorescent markers were excited at 442 nm (CFP) and 488 nm (GFP). Analysis of hypocotyls was performed on a time series acquired by sequential line scanning to minimize temporal variations. Additional confocal images were obtained using a Zeiss 710 equipped with 63× oil and 40× water objectives. A 561-nm diode laser was used for propidium iodide (Sigma) and RFP, a 488-nm laser was used for GFP, a 514-nm laser was used for YFP, and a 405-nm laser was used for CFP.

Image analysis was performed using a combination of software tools, ImageJ (version 1.36b; <http://rsbweb.nih.gov/ij/>), Image Pro Plus (Media Cybernetics), and Imaris (Bitplane). For the determination of vesicle trajectories and time-projected images, as recorded image sequences were enhanced by applying an alignment routine to the sequence to minimize drift, a flattening filter was used to correct for background artifacts and a bandpass filter to enhance small particles. For the time-projected images, more than 50 images were averaged, unless stated otherwise. Enhanced sequences were processed in Imaris by using an automated particle detection routine with a particle size of approximately 200 nm. Tracks were generated for these particles using appropriate gap and lifetime filters. Artifacts in the tracks data were eliminated manually. Data for the total displacement and duration for each track in a sequence were exported, average velocities were calculated, and histograms were plotted in Origin (OriginLab). Colocalization experiments were analyzed in 2d, using Imaris's automated colocalization tool on the basis of the algorithms described in detail earlier (Costes et al., 2004). Thresholds were

determined using the integrated wizard in Imaris, and three cells each, for the control and treated samples, were used. Each image sequence used contained between 13 and 30 frames.

MT images were observed for instances of MT tips leaving the cortex as described previously (Shaw et al., 2003). Videos using TUA5-RFP were obtained using the spinning disk as described above, cells were observed, and events of MT cortical disconnection were counted (in DMSO [*n* = 9 cells] and in CESTRIN [*n* = 12 cells]).

## Hypocotyl Growth Measurements

For growth analysis, seeds were sterilized, plated, cold vernalized, and germinated as described above; however, seedlings were germinated on plates containing 0.5× AGM with CESTRIN or isoxaben solubilized in DMSO. After 5 d, the plates were scanned using a flatbed scanner (Epson Perfection V300), and hypocotyl lengths were measured using the segmented line tool in the image-analysis software ImageJ (<http://imagej.nih.gov/ij/>). Statistical analyses were carried out using the statistical package R (<http://www.R-project.org>).

The Arabidopsis ecotype Col-0 was used in this study along with the mutants *ixr1-1* (Scheible et al., 2001) and *prc1-1* (Fagard et al., 2000).

## Escherichia coli Growth

Two milliliters of Luria-Bertani medium (10 g of tryptone, 5 g of yeast extract, 10 g of NaCl, and 1 L of distilled, deionized water, pH 7) was inoculated with a single colony of chemically competent *E. coli* TOP10 cells and incubated overnight at 37°C. Thirty microliters of this culture was then used to inoculate 3 mL of Luria-Bertani medium containing the chemical. The optimal density was measured every 30 min over 8 h using a spectrometer.

## Saccharomyces cerevisiae Growth

Two milliliters of liquid yeast extract peptone dextrose (YPD) medium (10 g of yeast extract, 20 g of peptone, 10 g of Glc [dextrose], and 1 L of distilled, deionized water, pH 7) was inoculated with a single colony of *S. cerevisiae* and incubated at 30°C for 24 h. Thirty microliters of yeast culture was added to 3 mL of fresh YPD medium and grown to an optimal density of 0.5. Plates were made with solid YPD (same as liquid with 1.5% [w/v] bacto agar) containing various concentrations of CESTRIN. The yeast culture was serially diluted (1:1, 1:10, 1:100, and 1:1,000), and 10 μL of each yeast concentration was spotted into each well of CESTRIN-containing medium. Plates were incubated in 30°C for 48 h.

## MT Polymerization Assay

The MT polymerization data were obtained using a polymerization assay kit (Cytoskeleton, Inc.), employing optimal density measurements of polymerized tubulin as described previously (Shelanski et al., 1973; Lee and Timasheff, 1977).

## Cellulose Content

Etiolated wild-type Col-0 Arabidopsis seedlings were grown on 0.5× AGM containing CESTRIN as described above. Hypocotyls were harvested after 8 d of growth. Cell wall materials were isolated into AIR (Günl et al., 2010), and cellulose content was estimated based on the principles of the modified Updegraff method (Updegraff, 1969). Briefly, the AIR remaining insoluble after a 1-h 2 N TFA hydrolysis at 121°C was collected by centrifugation and dissolved by stirring overnight at room temperature in 67% (v/v) sulfuric acid. Aliquots were then assayed using the anthrone colorimetric assay (Dische, 1962) with a 67% (v/v) sulfuric acid solution of cellulose powder (Whatman; CF11) used for the preparation of a standard curve.

## [<sup>13</sup>C]Glc Incorporation Assay and Analysis

Four-day-old etiolated Arabidopsis seedlings were germinated in liquid 0.5× MS medium containing 2% (w/v) Glc. Then the seedlings were grown in 0.5× MS liquid medium without Suc overnight prior to Glc chase. The etiolated seedlings were incubated for 2 h in 0.5× MS medium supplemented with 0.4% (w/v) <sup>13</sup>C-uniformly labeled Glc (Cambridge Isotope Laboratories) as the only sugar source and the indicated CESTRIN concentrations. After 2 h of

incubation, treated seedlings were washed three times to eliminate unincorporated Glc, and cell wall materials were extracted.

Cell wall materials were isolated into AIR (Günl et al., 2010). The AIR remaining insoluble after a 1-h 2 N TFA hydrolysis at 121°C (cellulose fraction) was collected by centrifugation, dissolved by stirring overnight in 15 N TFA at room temperature, and then hydrolyzed in 5 N TFA for 1 h. The 2 N and 15 N TFA fractions were derivatized into alditol acetates as described previously (Greve and Labavitch, 1991; Huysamer et al., 1997). Gas chromatography-mass spectrometry analysis was carried out as described previously in the selective ion monitoring mode to determine the relative incorporation of [<sup>15</sup>C] Glc. Secondary ions of 187 atomic mass units (from the <sup>12</sup>C precursor) and 191 atomic mass units (from the <sup>13</sup>C precursor) from the alditol acetates for Glc were used for quantification as described previously (Greve and Labavitch, 1991; Huysamer et al., 1997).

Sequence data in this article can be found in the Arabidopsis Genome Initiative database under the accession numbers POM2/CSI1 (At2g22125) and 3xYpet tag (6530483954; stock CD3-1727).

## Supplemental Data

The following supplemental materials are available.

**Supplemental Figure S1.** Structure of CESTRIN.

**Supplemental Figure S2.** The overall endomembrane morphology of etiolated hypocotyl cells is not noticeably affected under CESTRIN treatment.

**Supplemental Figure S3.** CESTRIN does not reduce growth of *E. coli*; however, growth reduction is observed in *S. cerevisiae*.

**Supplemental Figure S4.** Effect of CESTRIN treatment on the cytoskeleton.

**Supplemental Table S1.** Primer sequences used in generation of POM2/CSI1-3xYpet.

**Supplemental Movie S1.** GFP-CESA3 particle dynamics under DMSO treatment.

**Supplemental Movie S2.** GFP-CESA3 particle dynamics under CESTRIN (15 μM) treatment.

**Supplemental Movie S3.** Microtubule tip behavior (RFP-TUA5) under control, DMSO conditions.

**Supplemental Movie S4.** Microtubule tip behavior (RFP-TUA5) under CESTRIN (15 μM) treatment.

## ACKNOWLEDGMENTS

We thank Dr. Natasha Raikhel (University of California, Riverside) for generously sharing the 360 compound library, McKenzie Winter (University of California Davis) for assistance in screening mutants, Dr. Bo Liu (University of California, Davis) and Dr. Markus Pauly (University of California, Berkeley) for critical discussions, and Drs. Ian Moore (University of Oxford), Lorenzo Frigerio (University of Warwick), Niko Geldner (University of Lausanne), Chris Somerville (University of California, Berkeley), Andreas Nebenfur (University of Tennessee), Herman Hofte (National Institute of Agronomic Research, Versailles), Richard Cyr (Pennsylvania State University), Takashi Hashimoto (Nara Institute of Science and Technology, Japan), Karin Schumacher (Heidelberg University) and the Arabidopsis Biological Resource Center (Ohio State University) for sharing seed stocks of fluorescent markers and mutants. A patent application is pending to cover certain inventions described in the manuscript.

Received August 20, 2014; accepted December 17, 2014; published December 22, 2014.

## LITERATURE CITED

**Atmodjo MA, Hao Z, Mohnen D** (2013) Evolving views of pectin biosynthesis. *Annu Rev Plant Biol* **64**: 747–779

**Bashline L, Li S, Gu Y** (2014) The trafficking of the cellulose synthase complex in higher plants. *Ann Bot (Lond)* **114**: 1059–1067

**Baskin TI** (2001) On the alignment of cellulose microfibrils by cortical microtubules: a review and a model. *Protoplasma* **215**: 150–171

**Baskin TI** (2005) Anisotropic expansion of the plant cell wall. *Annu Rev Cell Dev Biol* **21**: 203–222

**Baskin TI, Beemster GT, Judy-March JE, Marga F** (2004) Disorganization of cortical microtubules stimulates tangential expansion and reduces the uniformity of cellulose microfibril alignment among cells in the root of Arabidopsis. *Plant Physiol* **135**: 2279–2290

**Bichet A, Desnos T, Turner S, Grandjean O, Höfte H** (2001) BOTERO1 is required for normal orientation of cortical microtubules and anisotropic cell expansion in Arabidopsis. *Plant J* **25**: 137–148

**Bischoff V, Cookson SJ, Wu S, Scheible WR** (2009) Thaxtomin A affects CESA-complex density, expression of cell wall genes, cell wall composition, and causes ectopic lignification in Arabidopsis thaliana seedlings. *J Exp Bot* **60**: 955–965

**Bischoff V, Desprez T, Mouille G, Vernhettes S, Gonneau M, Höfte H** (2011) Phytochrome regulation of cellulose synthesis in Arabidopsis. *Curr Biol* **21**: 1822–1827

**Brabham C, Debolt S** (2012) Chemical genetics to examine cellulose biosynthesis. *Front Plant Sci* **3**: 309

**Brabham C, Lei L, Gu Y, Stork J, Barrett M, DeBolt S** (2014) Indaziflam herbicidal action: a potent cellulose biosynthesis inhibitor. *Plant Physiol* **166**: 1177–1185

**Bringmann M, Li E, Sampathkumar A, Kocabek T, Hauser MT, Persson S** (2012) POM-POM2/cellulose synthase interacting1 is essential for the functional association of cellulose synthase and microtubules in Arabidopsis. *Plant Cell* **24**: 163–177

**Chan J, Calder GM, Doonan JH, Lloyd CW** (2003) EB1 reveals mobile microtubule nucleation sites in Arabidopsis. *Nat Cell Biol* **5**: 967–971

**Chen S, Ehrhardt DW, Somerville CR** (2010) Mutations of cellulose synthase (CESA1) phosphorylation sites modulate anisotropic cell expansion and bidirectional mobility of cellulose synthase. *Proc Natl Acad Sci USA* **107**: 17188–17193

**Costes SV, Daelemans D, Cho EH, Dobbin Z, Pavlakis G, Lockett S** (2004) Automatic and quantitative measurement of protein-protein colocalization in live cells. *Biophys J* **86**: 3993–4003

**Crowell EF, Bischoff V, Desprez T, Rolland A, Stierhof YD, Schumacher K, Gonneau M, Höfte H, Vernhettes S** (2009) Pausing of Golgi bodies on microtubules regulates secretion of cellulose synthase complexes in Arabidopsis. *Plant Cell* **21**: 1141–1154

**DeBolt S, Gutierrez R, Ehrhardt DW, Melo CV, Ross L, Cutler SR, Somerville C, Bonetta D** (2007a) Morlin, an inhibitor of cortical microtubule dynamics and cellulose synthase movement. *Proc Natl Acad Sci USA* **104**: 5854–5859

**DeBolt S, Gutierrez R, Ehrhardt DW, Somerville C** (2007b) Nonmotile cellulose synthase subunits repeatedly accumulate within localized regions at the plasma membrane in Arabidopsis hypocotyl cells following 2,6-dichlorobenzonitrile treatment. *Plant Physiol* **145**: 334–338

**Desprez T, Juraniec M, Crowell EF, Jouy H, Pochylova Z, Parcy F, Höfte H, Gonneau M, Vernhettes S** (2007) Organization of cellulose synthase complexes involved in primary cell wall synthesis in Arabidopsis thaliana. *Proc Natl Acad Sci USA* **104**: 15572–15577

**Detmer J, Hong-Hermesdorf A, Stierhof YD, Schumacher K** (2006) Vacuolar H<sup>+</sup>-ATPase activity is required for endocytic and secretory trafficking in Arabidopsis. *Plant Cell* **18**: 715–730

**Dische Z** (1962) Color reaction of carbohydrates. In R Whistler, M Wolfson, eds, *Methods in Carbohydrate Biochemistry*. Academic Press, New York, pp 475–514

**Dixit R, Chang E, Cyr R** (2006) Establishment of polarity during organization of the acentrosomal plant cortical microtubule array. *Mol Biol Cell* **17**: 1298–1305

**Drakakaki G, Robert S, Raikhel NV, Hicks GR** (2009) Chemical dissection of endosomal pathways. *Plant Signal Behav* **4**: 57–62

**Drakakaki G, Robert S, Szatmari AM, Brown MQ, Nagawa S, Van Damme D, Leonard M, Yang Z, Girke T, Schmid SL, et al** (2011) Clusters of bioactive compounds target dynamic endomembrane networks in vivo. *Proc Natl Acad Sci USA* **108**: 17850–17855

**Drakakaki G, van de Ven W, Pan S, Miao Y, Wang J, Keinath NF, Weatherly B, Jiang L, Schumacher K, Hicks G, et al** (2012) Isolation and proteomic analysis of the SYP61 compartment reveal its role in exocytic trafficking in Arabidopsis. *Cell Res* **22**: 413–424

**Dunkley TP, Hester S, Shadforth IP, Runions J, Weimar T, Hanton SL, Griffin JL, Bessant C, Brandizzi F, Hawes C, et al** (2006) Mapping the Arabidopsis organelle proteome. *Proc Natl Acad Sci USA* **103**: 6518–6523

- Fagard M, Desnos T, Desprez T, Goubet F, Refregier G, Mouille G, McCann M, Rayon C, Vernhettes S, Höfte H (2000) *PROCUSTE1* encodes a cellulose synthase required for normal cell elongation specifically in roots and dark-grown hypocotyls of *Arabidopsis*. *Plant Cell* **12**: 2409–2424
- Fernandes AN, Thomas LH, Altaner CM, Callow P, Forsyth VT, Apperley DC, Kennedy CJ, Jarvis MC (2011) Nanostructure of cellulose microfibrils in spruce wood. *Proc Natl Acad Sci USA* **108**: E1195–E1203
- Gardiner JC, Taylor NG, Turner SR (2003) Control of cellulose synthase complex localization in developing xylem. *Plant Cell* **15**: 1740–1748
- Geldner N, Déneraud-Tendon V, Hyman DL, Mayer U, Stierhof YD, Chory J (2009) Rapid, combinatorial analysis of membrane compartments in intact plants with a multicolor marker set. *Plant J* **59**: 169–178
- Green PB (1962) Mechanism for plant cellular morphogenesis. *Science* **138**: 1404–1405
- Greve LC, Labavitch JM (1991) Cell wall metabolism in ripening fruit: V. Analysis of cell wall synthesis in ripening tomato pericarp tissue using a  $D$ -[ $^{13}C$ ]glucose tracer and gas chromatography-mass spectrometry. *Plant Physiol* **97**: 1456–1461
- Groen AJ, Sancho-Andrés G, Breckels LM, Gatto L, Aniento F, Lilley KS (2014) Identification of trans-Golgi network proteins in *Arabidopsis thaliana* root tissue. *J Proteome Res* **13**: 763–776
- Gu Y, Kaplinsky N, Bringham M, Cobb A, Carroll A, Sampathkumar A, Baskin TI, Persson S, Somerville CR (2010) Identification of a cellulose synthase-associated protein required for cellulose biosynthesis. *Proc Natl Acad Sci USA* **107**: 12866–12871
- Günl M, Gille S, Pauly M (2010) OLIGO Mass Profiling (OLIMP) of extracellular polysaccharides. *J Vis Exp* **40**: 2046
- Gutierrez R, Lindeboom JJ, Paredes AR, Emons AM, Ehrhardt DW (2009) *Arabidopsis* cortical microtubules position cellulose synthase delivery to the plasma membrane and interact with cellulose synthase trafficking compartments. *Nat Cell Biol* **11**: 797–806
- Haigler CH, Brown RM (1986) Transport of rosettes from the Golgi apparatus to the plasma membrane in isolated mesophyll cells of *Zinnia elegans* during differentiation to tracheary elements in suspension culture. *Protoplasma* **134**: 111–120
- Harris DM, Corbin K, Wang T, Gutierrez R, Bertolo AL, Petti C, Smilgies DM, Estevez JM, Bonetta D, Urbanowicz BR, et al (2012) Cellulose microfibril crystallinity is reduced by mutating C-terminal transmembrane region residues CESA1A903V and CESA3T942I of cellulose synthase. *Proc Natl Acad Sci USA* **109**: 4098–4103
- Heim DR, Roberts JL, Pike PD, Larrinua IM (1989) Mutation of a locus of *Arabidopsis thaliana* confers resistance to the herbicide isoxaben. *Plant Physiol* **90**: 146–150
- Hématy K, Sado PE, Van Tuinen A, Rochange S, Desnos T, Balzergue S, Pelletier S, Renou JP, Höfte H (2007) A receptor-like kinase mediates the response of *Arabidopsis* cells to the inhibition of cellulose synthesis. *Curr Biol* **17**: 922–931
- Herth W (1987) Effects of 2,6-DCB on plasma membrane rosettes of wheat root cells. *Naturwissenschaften* **74**: 556–557
- Hunter PR, Craddock CP, Di Benedetto S, Roberts LM, Frigerio L (2007) Fluorescent reporter proteins for the tonoplast and the vacuolar lumen identify a single vacuolar compartment in *Arabidopsis* cells. *Plant Physiol* **145**: 1371–1382
- Huysamer M, Greve LC, Labavitch JM (1997) Cell wall metabolism in ripening fruit: IX. Synthesis of pectic and hemicellulosic cell wall polymers in the outer pericarp of mature green tomatoes (cv XMT-22). *Plant Physiol* **114**: 1523–1531
- Jarvis MC (2013) Cellulose biosynthesis: counting the chains. *Plant Physiol* **163**: 1485–1486
- Konopka CA, Backues SK, Bednarek SY (2008) Dynamics of *Arabidopsis* dynamin-related protein 1C and a clathrin light chain at the plasma membrane. *Plant Cell* **20**: 1363–1380
- Landrein B, Lathe R, Bringmann M, Vuillot C, Ivakov A, Boudaoud A, Persson S, Hamant O (2013) Impaired cellulose synthase guidance leads to stem torsion and twists phyllotactic patterns in *Arabidopsis*. *Curr Biol* **23**: 895–900
- Lane DR, Wiedemeier A, Peng L, Höfte H, Vernhettes S, Desprez T, Hocart CH, Birch RJ, Baskin TI, Burn JE, et al (2001) Temperature-sensitive alleles of *RSW2* link the *KORRIGAN* endo-1,4- $\beta$ -glucanase to cellulose synthesis and cytokinesis in *Arabidopsis*. *Plant Physiol* **126**: 278–288
- Ledbetter MC, Porter KR (1963) A “microtubule” in plant cell fine structure. *J Cell Biol* **19**: 239–250
- Lee JC, Timasheff SN (1977) In vitro reconstitution of calf brain microtubules: effects of solution variables. *Biochemistry* **16**: 1754–1764
- Lei L, Li S, Bashline L, Gu Y (2014a) Dissecting the molecular mechanism underlying the intimate relationship between cellulose microfibrils and cortical microtubules. *Front Plant Sci* **5**: 90
- Lei L, Zhang T, Strasser R, Lee CM, Gonneau M, Mach L, Vernhettes S, Kim SH, Cosgrove D, Li S, et al (2014b) The *jaoyao1* mutant is an allele of *korrigan1* that abolishes endoglucanase activity and affects the organization of both cellulose microfibrils and microtubules in *Arabidopsis*. *Plant Cell* **26**: 2601–2616
- Li S, Lei L, Somerville CR, Gu Y (2012) Cellulose synthase interactive protein 1 (CSII) links microtubules and cellulose synthase complexes. *Proc Natl Acad Sci USA* **109**: 185–190
- Mathur J, Spielhofer P, Kost B, Chua N (1999) The actin cytoskeleton is required to elaborate and maintain spatial patterning during trichome cell morphogenesis in *Arabidopsis thaliana*. *Development* **126**: 5559–5568
- McFarlane HE, Döring A, Persson S (2014) The cell biology of cellulose synthesis. *Annu Rev Plant Biol* **65**: 69–94
- Mei Y, Gao HB, Yuan M, Xue HW (2012) The *Arabidopsis* ARCP protein, CSII, which is required for microtubule stability, is necessary for root and anther development. *Plant Cell* **24**: 1066–1080
- Morejohn LC, Bureau TE, Molè-Bajer J, Bajer AS, Fosket DE (1987) Oryzalin, a dinitroaniline herbicide, binds to plant tubulin and inhibits microtubule polymerization in vitro. *Planta* **172**: 252–264
- Mutwil M, Debolt S, Persson S (2008) Cellulose synthesis: a complex complex. *Curr Opin Plant Biol* **11**: 252–257
- Nakamura M, Naoi K, Shoji T, Hashimoto T (2004) Low concentrations of propyzamide and oryzalin alter microtubule dynamics in *Arabidopsis* epidermal cells. *Plant Cell Physiol* **45**: 1330–1334
- Nebenführ A, Gallagher LA, Dunahay TG, Frohlich JA, Mazurkiewicz AM, Meehl JB, Staehelin LA (1999) Stop-and-go movements of plant Golgi stacks are mediated by the actomyosin system. *Plant Physiol* **121**: 1127–1142
- Nelson BK, Cai X, Nebenführ A (2007) A multicolored set of in vivo organelle markers for co-localization studies in *Arabidopsis* and other plants. *Plant J* **51**: 1126–1136
- Newman RH, Hill SJ, Harris PJ (2013) Wide-angle x-ray scattering and solid-state nuclear magnetic resonance data combined to test models for cellulose microfibrils in mung bean cell walls. *Plant Physiol* **163**: 1558–1567
- Nikolovski N, Rubtsov D, Segura MP, Miles GP, Stevens TJ, Dunkley TP, Munro S, Lilley KS, Dupree P (2012) Putative glycosyltransferases and other plant Golgi apparatus proteins are revealed by LOPIT proteomics. *Plant Physiol* **160**: 1037–1051
- Paredes AR, Persson S, Ehrhardt DW, Somerville CR (2008) Genetic evidence that cellulose synthase activity influences microtubule cortical array organization. *Plant Physiol* **147**: 1723–1734
- Paredes AR, Somerville CR, Ehrhardt DW (2006) Visualization of cellulose synthase demonstrates functional association with microtubules. *Science* **312**: 1491–1495
- Parsons HT, Christiansen K, Knierim B, Carroll A, Ito J, Bath TS, Smith-Moritz AM, Morrison S, McInerney P, Hadi MZ, et al (2012) Isolation and proteomic characterization of the *Arabidopsis* Golgi defines functional and novel components involved in plant cell wall biosynthesis. *Plant Physiol* **159**: 12–26
- Persson S, Paredes A, Carroll A, Palsdottir H, Doblin M, Poindexter P, Khitrov N, Auer M, Somerville CR (2007) Genetic evidence for three unique components in primary cell-wall cellulose synthase complexes in *Arabidopsis*. *Proc Natl Acad Sci USA* **104**: 15566–15571
- Robert S, Bichet A, Grandjean O, Kierzkowski D, Satiat-Jeunemaître B, Pelletier S, Hauser MT, Höfte H, Vernhettes S (2005) An *Arabidopsis* endo-1,4- $\beta$ -D-glucanase involved in cellulose synthesis undergoes regulated intracellular cycling. *Plant Cell* **17**: 3378–3389
- Robert S, Chary SN, Drakakaki G, Li S, Yang Z, Raikhel NV, Hicks GR (2008) Endosidin1 defines a compartment involved in endocytosis of the brassinosteroid receptor BRI1 and the auxin transporters PIN2 and AUX1. *Proc Natl Acad Sci USA* **105**: 8464–8469
- Roudier F, Fernandez AG, Fujita M, Himmelspach R, Borner GH, Schindelman G, Song S, Baskin TI, Dupree P, Wasteneys GO, et al (2005) COBRA, an *Arabidopsis* extracellular glycosyl-phosphatidyl inositol-anchored protein, specifically controls highly anisotropic expansion through its involvement in cellulose microfibril orientation. *Plant Cell* **17**: 1749–1763

- Sampathkumar A, Gutierrez R, McFarlane HE, Bringmann M, Lindeboom J, Emons AM, Samuels L, Ketelaar T, Ehrhardt DW, Persson S** (2013) Patterning and lifetime of plasma membrane-localized cellulose synthase is dependent on actin organization in Arabidopsis interphase cells. *Plant Physiol* **162**: 675–688
- Scheible WR, Eshed R, Richmond T, Delmer D, Somerville C** (2001) Modifications of cellulose synthase confer resistance to isoxaben and thiazolidinone herbicides in Arabidopsis *Ixr1* mutants. *Proc Natl Acad Sci USA* **98**: 10079–10084
- Scheller HV, Ulvskov P** (2010) Hemicelluloses. *Annu Rev Plant Biol* **61**: 263–289
- Shaw SL, Kamyar R, Ehrhardt DW** (2003) Sustained microtubule treadmill in Arabidopsis cortical arrays. *Science* **300**: 1715–1718
- Shelanski ML, Gaskin F, Cantor CR** (1973) Microtubule assembly in the absence of added nucleotides. *Proc Natl Acad Sci USA* **70**: 765–768
- Smertenko AP, Chang HY, Sonobe S, Fenyk SI, Weingartner M, Bögre L, Hussey PJ** (2006) Control of the AtMAP65-1 interaction with microtubules through the cell cycle. *J Cell Sci* **119**: 3227–3237
- Smertenko AP, Kaloriti D, Chang HY, Fiserova J, Opatrny Z, Hussey PJ** (2008) The C-terminal variable region specifies the dynamic properties of *Arabidopsis* microtubule-associated protein MAP65 isotypes. *Plant Cell* **20**: 3346–3358
- Somerville C** (2006) Cellulose synthesis in higher plants. *Annu Rev Cell Dev Biol* **22**: 53–78
- Sugimoto K, Himmelspach R, Williamson RE, Wasteneys GO** (2003) Mutation or drug-dependent microtubule disruption causes radial swelling without altering parallel cellulose microfibril deposition in *Arabidopsis* root cells. *Plant Cell* **15**: 1414–1429
- Thomas LH, Forsyth VT, Sturcová A, Kennedy CJ, May RP, Altaner CM, Apperley DC, Wess TJ, Jarvis MC** (2013) Structure of cellulose microfibrils in primary cell walls from collenchyma. *Plant Physiol* **161**: 465–476
- Updegraff DM** (1969) Semimicro determination of cellulose in biological materials. *Anal Biochem* **32**: 420–424
- Vain T, Crowell EF, Timpano H, Biot E, Desprez T, Mansoori N, Trindade LM, Pagant S, Robert S, Höfte H, et al** (2014) The cellulase KORRIGAN is part of the cellulose synthase complex. *Plant Physiol* **165**: 1521–1532
- Wasteneys GO, Fujita M** (2006) Establishing and maintaining axial growth: wall mechanical properties and the cytoskeleton. *J Plant Res* **119**: 5–10
- Yoneda A, Higaki T, Kutsuna N, Kondo Y, Osada H, Hasezawa S, Matsui M** (2007) Chemical genetic screening identifies a novel inhibitor of parallel alignment of cortical microtubules and cellulose microfibrils. *Plant Cell Physiol* **48**: 1393–1403
- Yoneda A, Ito T, Higaki T, Kutsuna N, Saito T, Ishimizu T, Osada H, Hasezawa S, Matsui M, Demura T** (2010) Cobtorin target analysis reveals that pectin functions in the deposition of cellulose microfibrils in parallel with cortical microtubules. *Plant J* **64**: 657–667
- Zhou R, Benavente LM, Stepanova AN, Alonso JM** (2011) A recombineering-based gene tagging system for Arabidopsis. *Plant J* **66**: 712–723
- Zheng H, Kunst L, Hawes C, Moore I** (2004) A GFP-based assay reveals a role for RHD3 in transport between the endoplasmic reticulum and Golgi apparatus. *Plant J* **37**: 398–414